Journal of
Materials Chemistry B

COMMUNICATION

Cite this: DOI: 10.1039/c7tb00623c

Received 7th March 2017,
Accepted 9th June 2017

DOI: 10.1039/c7tb00623c

rsc.li/materials-b

Modulating aggregation-induced emission *via* a non-conjugated linkage of fluorophores to tetraphenylethenes†

Xie Han,[a] Bibo Zhang,[b] Jianhua Chen,[a] Sheng Hua Liu,[a] Chunyan Tan,[b] Haiyang Liu,[b] Matthew J. Lang,[cd] Ying Tan,*[b] Xiaogang Liu*[ce] and Jun Yin*[ab]

A fluorophore consisting of two fluorescent moieties could display unusual optical behaviors that are unattainable in a single-fluorophore compound. Herein we reported two "dual-fluorophore" dyes: DNS-linked tetraphenylethene demonstrates bright aggregation-induced emission, while NBD-linked tetraphenylethene exhibits aggregation-caused quenching. Our results have important implications for engineering emission behaviors of molecular aggregates for practical applications.

The exploitation of highly emissive fluorescent dyes has attracted considerable research interests, owing to their broad applications in photoelectronic materials,[1] biological sensors,[2] chemosensors,[3] luminescent materials,[4] and so on. However, most of the organic fluorescent dyes are weakly emissive or non-emissive in the solid state due to the notorious aggregation caused quenching (ACQ) effect.[5] In contrast, Tang's group discovered an aggregation induced emission (AIE) phenomenon which is exactly opposite to ACQ.[6] Since then, various AIE compounds, many of which are conjugated tetraphenylethene (**TPE**) derivatives, have been reported and used in numerous applications.[7,8]

Recently, **TPE** backbones have been expanded *via* non-conjugated incorporation of other fluorescent dyes, such as rhodamine[9] and borondipyrromethene (BODIPY),[10] to further adjust their optical behaviors for different applications. For example, Jia and Ma *et al.* linked a rhodamine compound to **TPE** *via* an amino-containing alkyl chain. The resulting compound showed a mechanochromic fluorescence with a sequential tricolor change upon grinding.[9d] Liu *et al.* synthesized a rhodamine-modified **TPE** derivative containing a tumor-targeting RGD peptide; this compound could be used to monitor the generation of singlet oxygen during the photodynamic ablation of tumor cells.[9f]

In this communication, we demonstrate that the AIE behaviours of **TPE** could be effectively adjusted *via* the non-conjugated linkage of one additional fluorophore. We have attached two commercially available dyes, a dansyl dye (**DNS**) and 4-methylamino-7-nitrobenzo-2,1,3-oxadiazole (**NBD**), to **TPE** (Scheme 1). Our results show that the fluorescence intensity of **TPE-DNS** experienced a slight decrease, followed by a significantly AIE induced enhancement, as the ratio of water content increases in the acetonitrile–water binary mixture. In contrast, **TPE-NBD** displayed a monotonous drop in the emission intensity and an ACQ characteristic as more water was added. We have analysed the underlying mechanism for these distinct behaviours *via* both experimental measurements and quantum chemical calculations based on (time-dependent) density functional theory [(TD)-DFT]. In addition, we have demonstrated that both

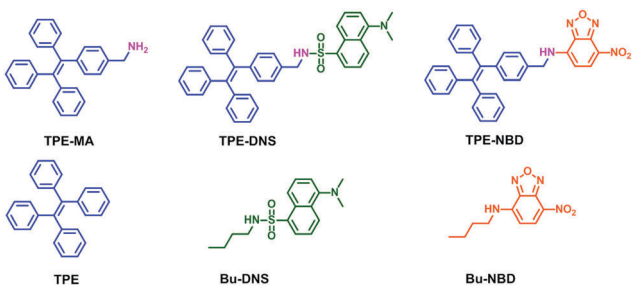

Scheme 1 The structures of compounds **TPE-MA**, **TPE-DNS**, **TPE-NBD**, **TPE**, **Bu-DNS** and **Bu-NBD**.

[a] Key Laboratory of Pesticide and Chemical Biology, Ministry of Education, College of Chemistry, Central China Normal University, Wuhan 430079, China. E-mail: yinj@mail.ccnu.edu.cn
[b] The Ministry-Province Jointly Constructed Base for State Key Lab-Shenzhen Key Laboratory of Chemical Biology, the Graduate School at Shenzhen, Tsinghua University, Shenzhen, Guangdong 518055, China. E-mail: tan.ying@sz.tsinghua.edu.cn
[c] Singapore-MIT Alliance for Research and Technology (SMART), 1 CREATE Way, Singapore 138602, Singapore. E-mail: xiaogang@smart.mit.edu
[d] Department of Chemical and Biomolecular Engineering and Department of Molecular Physiology and Biophysics, Vanderbilt University, Nashville, Tennessee 37235, USA
[e] Singapore University of Technology and Design, 8 Somapah Road, Singapore 487372, Singapore. E-mail: xiaogang_liu@sutd.edu.sg

† Electronic supplementary information (ESI) available: Synthesis, characterization, experimental and computational details, and crystallographic information files. CCDC 1548388 and 1548389. For ESI and crystallographic data in CIF or other electronic format see DOI: 10.1039/c7tb00623c

TPE-DNS and **TPE-NBD** showed good biocompatibility for live cell imaging.

We synthesized **TPE-DNS** and **TPE-NBD** *via* a one-step reaction of (4-(1,2,2-triphenylvinyl)phenyl)methanamine (**TPE-MA**) with dansyl chloride (**DNS-Cl**) or 4-chloride-7-nitrobenzo-2,1,3-oxadiazole (**NBD-Cl**) in the presence of Et_3N, respectively (yields: 30–53%). The amine group in **TPE-MA** allows easy linkage of other fluorophores to **TPE** (Scheme 1).[11] And the synthesis of **TPE-MA**, a key intermediate in this reaction, was reported in our previous work.[12]

After that, we studied AIE behaviors of **TPE-DNS** and **TPE-NBD** in the binary mixture of CH_3CN and water. The UV-Vis absorption spectra of **TPE-DNS** exhibit the main absorption band peaked at ~305 nm (Fig. S1A, ESI†). This absorption band resulted from the overlapping absorptions from both **TPE** and **DNS** moieties, as reflected by the UV-Vis absorption spectra of two reference compounds—**TPE** and **Bu-DNS** (Scheme 1 and Fig. S2A, S3A, ESI†).[12b,e] Indeed, time-dependent density functional theory (TD-DFT) calculations predict two intense and close absorption transitions for **TPE-DNS** in acetonitrile at ~344 and ~380 nm, respectively (Fig. S5 and Table S1, ESI†). The first transition (dominated by HOMO → LUMO+1) was mainly assigned to the **TPE** moiety whereas the electron densities involved in the second transition (dominated by HOMO−1 → LUMO) were largely delocalized in the **DNS** unit. In contrast, **TPE-NBD** displayed two distinct absorption bands, peaked at ~459 nm and ~346 nm, respectively (Fig. S1B, ESI†). These two peaks are attributed to the absorption of **NBD** and **TPE** fragments, respectively, according to our studies on reference compounds **TPE** and **Bu-NBD** as well as TD-DFT calculations (Scheme 1, Fig. S2A, S6A and Table S1, ESI†).[12b–d] Nevertheless, no obvious shifts in the UV-Vis absorption spectra of **TPE-DNS** and **TPE-NBD** were observed when we varied the volume fractions of water (f_W) in the CH_3CN–water mixture.

The AIE behavior of **TPE-DNS** was clearly demonstrated in its fluorescence spectra. The emission peaks of **TPE-DNS** exhibited a complicated solvatochromic shift (Fig. 1a). In pure CH_3CN, **TPE-DNS** displayed a yellow-green fluorescence at ~509 nm and the absolute fluorescence quantum yield was 32.4%. With increasing f_W, the emission intensity of **TPE-DNS** gradually decreased in conjunction with a red-shift in the peak emission wavelengths and the absolute fluorescence quantum yield showed a slight reduction (from 32.4% to 28.6%) (Fig. 1b and c). The red shift is mainly due to the intramolecular charge transfer (ICT) effect of the **DNS** moiety in response to the increasing solvent polarity of the CH_3CN–water mixture, as f_W increases from 0 to 60% (Fig. S3B and S4A, ESI†). When f_W increased to >60%, the emission intensity of **TPE-DNS** increased dramatically. Simultaneously, the emission peak experienced a blue-shift from 537 to 492 nm with enhanced fluorescence quantum yields of up to 94.1% (Fig. 1a and b); the emission color changed from yellow to blue-green (Fig. 1c). We attributed the intensification and blue shift of **TPE-DNS** emissions to considerable molecular aggregation and AIE, resulting from the **TPE** moiety (Fig. S2B, ESI†). The formation of molecular aggregates was further proved by dynamic light scattering

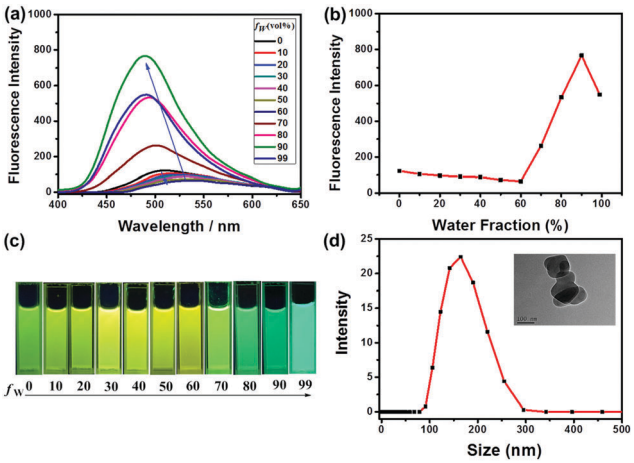

Fig. 1 (a) Fluorescence spectra of **TPE-DNS** (10 μM) in the acetonitrile–water binary mixture with different water fractions (f_W). (b) Plot of peak fluorescence intensities of **TPE-DNS** (10 μM) in the acetonitrile–water mixture. (c) Fluorescence images of **TPE-DNS** in acetonitrile–water with different water fractions (λ_{ex} = 340 nm; slit: 15/2.5 nm). (d) Particle size distributions of **TPE-DNS** in the binary mixture of acetonitrile (10%) and water (90%), as measured by dynamic light scattering (DLS); inset: TEM image of the nanoaggregates of **TPE-DNS** formed in an acetonitrile–water mixture with 90% water fraction.

(DLS) and transmission electron microscopy (TEM) (Fig. 1d and Fig. S7, ESI†). For example, the effective diameter of TPE-DNS aggregates amounts to ~156 nm in the acetonitrile–water mixture (Fig. 1d). In comparison to the aggregation turn-on threshold of **TPE-DNS** (f_W = 60%), the aggregation of **TPE** (the reference compound) becomes apparent only when f_W increases to 80% (Fig. S2, ESI†). These results suggested that the introduction of a **DNS** fluorophore reduces the solubility of **TPE-DNS** and lowers the AIE turn-off threshold to a small f_W value.

In contrast, **TPE-NBD** displayed a different aggregation behaviour. **TPE-NBD** showed a green emission peaked at 520 nm in pure CH_3CN and the absolute fluorescence quantum yield was 1.6% (due to the emission of the NBD moiety, excited at 450 nm). Along with increasing f_W, the emission intensity of **TPE-NBD** gradually decreased and the fluorescence quantum yield dropped to 0.9%, in conjunction with a red-shift from 520 nm to 554 nm (Fig. 2). This change in fluorescence colors is partly attributed to the ICT effect of the **NBD** moiety (Fig. S4B and S6, ESI†). Similarly, the drop of fluorescence intensities in more aqueous solvents (with increasing f_W) is partially related to the intensive hydrogen bond interactions around the monomers of the **NBD** moiety.[13] Interestingly, by varying f_W from 0 to 99%, we did not observe a noticeable AIE emission of the **TPE** moiety throughout the course (even when excited at 340 nm; Fig. S8, ESI†).

Although there is a lack of noticeable AIE emissions from the **TPE** moiety, both DLS experiments and TEM images clearly proved the formation of molecular aggregates in the **TPE-NBD** solution when the water fraction reached 90% (Fig. 2d and Fig. S7B, ESI†). The absence of **TPE** emissions in these aggregates is likely caused by efficient Förster resonance energy transfer from the **TPE** to the **NBD** moieties (Fig. S2B and S6A, ESI†). Moreover, although considerable energy is transferred to

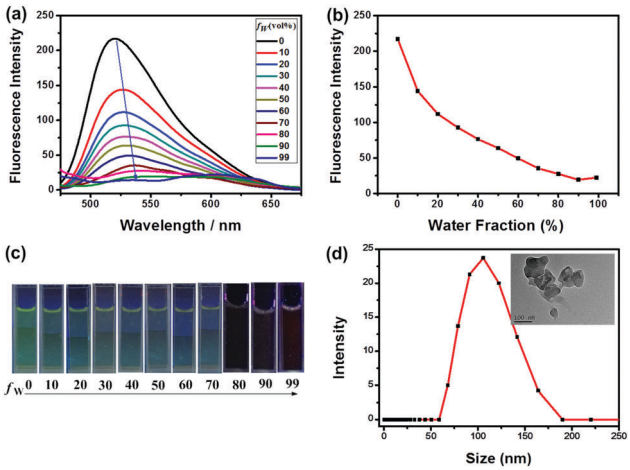

Fig. 2 (a) Fluorescence spectra of **TPE-NBD** (10 μM) in the acetonitrile–water binary mixture with different water fractions (f_W). (b) Plot of peak fluorescence intensities of **TPE-NBD** (10 μM) in the acetonitrile–water mixture. (c) Fluorescence images of **TPE-NBD** in acetonitrile–water with different water fractions (λ_{ex} = 450 nm; slit: 10/5 nm). (d) Particle size distributions of **TPE-NBD** in the binary mixture of acetonitrile (10%) and water (90%), as measured by dynamic light scattering (DLS); inset: TEM image of the nanoaggregates of **TPE-NBD** formed in an acetonitrile–water mixture with 90% water fraction.

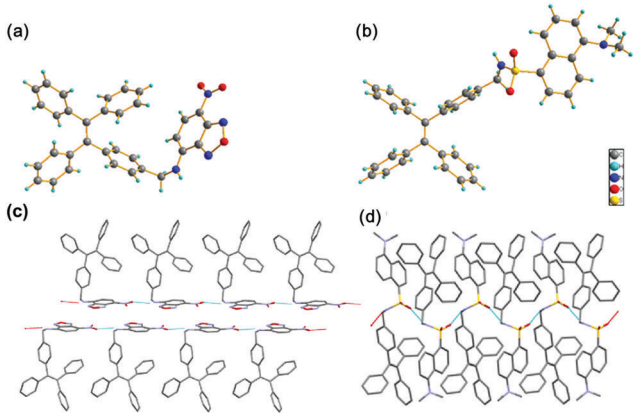

Fig. 3 The crystal structures of **TPE-NBD** (a), **TPE-DNS** (b) and the packing view of **TPE-NBD** (c) and **TPE-DNS** (d). Hydrogen bonds are denoted with blue dotted lines, while hydrogen atoms are omitted in (c) and (d) for clarity.

the **NBD** moiety, the fluorescence of **NBD** seems to be significantly quenched in **TPE-NBD** aggregates.

An efficient energy transfer from **TPE** to **NBD** moieties in **TPE-NBD** was further proved by physically mixing **TPE** and **Bu-NBD** in the acetonitrile–water solution (Fig. S9, ESI†). The average distance between **TPE** and **NBD** moieties becomes larger in the physical mixture than that in **TPE-NBD**, thereby suppressing the potential energy transfer. Indeed, we observed a weak emission peak due to the **TPE** aggregates at ∼450 nm in the physical mixture, when f_W increased to >60%. The appearance of this peak fully matches incomplete energy transfer from **TPE** to **Bu-NBD** in the physical mixture.

The starkly different emission characteristics of **TPE-NBD** and **TPE-DNS** aggregates also motivated us to explore their intermolecular interactions in the solid state. We obtained the crystal structures of **TPE-DNS** and **TPE-NBD** *via* X-ray diffraction experiments (Fig. 3a, b and Tables S2, S3, ESI†). In packed **TPE-NBD** molecules, strong hydrogen bond interactions connected the neighbouring **NBD** moieties in a head-to-tail (and J-aggregate like) manner (O···H–N distance: 2.888 Å; Fig. 3c). The strong dipole–dipole interactions between these polar **NBD** moieties lead to significantly red-shifted emissions peaked at 592 nm in the solid state (Fig. S10, ESI†), in comparison to ∼520 nm in acetonitrile. Besides, we noticed weak π–π stacking interactions between the two layers of NBD moieties (Fig. S11, ESI†). Consequently, intermolecular hydrogen bond and π–π stacking interactions greatly reduce the emission intensities, making **TPE-NBD** an ACQ compound.[14]

Likewise, hydrogen bond interactions are also present between the **DNS** moieties in the **TPE-DNS** crystal (O···H–N distance: 2.840 Å; Fig. 3d), but no π–π stacking interactions are observed. These hydrogen bond interactions could diminish the fluorescence of **DNS**. Nevertheless, there is a lack of efficient FRET from **TPE** to **DNS**, due to the mismatch between the **TPE** emission and **DNS** absorption spectra. Consequently, bright emissions from the aggregated **TPE** moieties endow **TPE-DNS** with an AIE characteristic. A similar AIE phenomenon is also observed in the physical mixture of **TPE** and **Bu-DNS**, due to the AIE of **TPE** molecules (Fig. S9, ESI†).

On account of the fluorescence properties of **TPE-DNS** and **TPE-NBD**, we applied them in bioimaging of live cells. Firstly, the cytotoxicity of **TPE-DNS** and **TPE-NBD** at different concentrations was evaluated by using the 3-(4,5-dimethylthiazol-2-yl)-2,5-diphenyltetrazolium bromide (MTT) assay in HeLa cells. Both **TPE-DNS** and **TPE-NBD** exhibited low cellular toxicity and good biocompatibility. After 24 hours of incubation, the cell viability of HeLa cells remains at >88% at dye concentrations of up to 10 μM and at >83% at dye concentrations of up to 200 μM (Fig. S12, ESI†).

Next, we incubated HeLa cells in **TPE-DNS** and **TPE-NBD** solutions (5 μM) at 37 °C for different durations (0, 15, 30, 45, and 60 min), and then washed these cells with PBS. The fluorescence images were collected using a confocal microscope (LCFM). In cells stained with **TPE-DNS** and **TPE-NBD**, weak emissions were detected after 15 min of incubation, mainly in the cytoplasm of HeLa cells (Fig. 4 and Fig. S13, ESI†). Moreover, the fluorescence intensity gradually increased at a longer incubation time. Overall, these bioimaging experiments indicated that **TPE-NBD** and **TPE-DNS** had good cell permeability, and could be deployed in fluorescence bioimaging.

In conclusion, based on **TPE-MA** and its facile reaction, we demonstrate that the AIE effect is adjustable *via* a non-conjugated linkage of tetraphenylethene (**TPE**) to another fluorescent moiety (*i.e.*, **DNS** or **NBD**). We find that **TPE-DNS** demonstrates a higher tendency to molecular aggregation than unsubstituted **TPE** and displays a bright AIE. In contrast, **TPE-NBD** exhibited aggregation caused quenching (ACQ), due to an efficient energy transfer from **TPE** to **NBD** moieties and strong intermolecular interactions between **NBD** moieties. Finally, both **TPE-DNS** and **TPE-NBD** involve simple synthesis

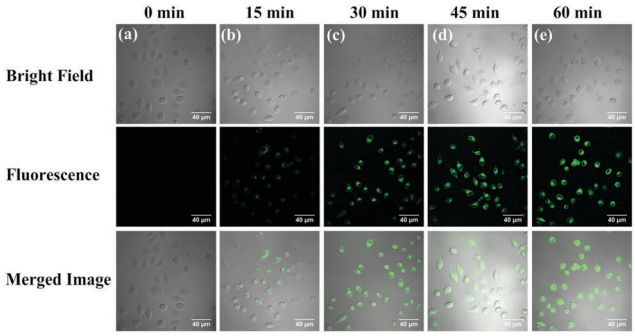

Fig. 4 Confocal microscope images of HeLa cells in the presence of **TPE-DNS** (5 μM): (a) the cells incubated with **TPE-DNS** for 0 min; (b) the cells incubated with **TPE-DNS** for 15 min; (c) the cells incubated with **TPE-DNS** for 30 min; (d) the cells incubated with **TPE-DNS** for 45 min; and (e) the cells incubated with **TPE-DNS** for 60 min.

and exhibit excellent biocompatibility and cell permeability in bioimaging of live cells. We expect that our strategy provides new insights into modulation of AIE behaviors of TPE-based materials for fluorescence applications.

The authors acknowledge financial support from the National Natural Science Foundation of China (21676113, 21402057, 21472059); the Youth Chen-Guang Project of Wuhan (2016070204010098); self-determined research funds of CCNU from the colleges' basic research and operation of MOE (CCNU16A02004); the excellent doctoral dissertation cultivation grant from the Central China Normal University (2016YBZZ019); and facilitation from the Ministry-Province Jointly Constructed Base for State Key Lab at Shenzhen Key Laboratory of Chemical Biology, China. X. L. and M. J. L. are thankful for financial support from the National Research Foundation of Singapore (through Singapore-MIT Alliance for Research and Technology). X. L. is indebted to Singapore University of Technology and Design for a Startup Research Grant.

Notes and references

1 (*a*) J. Wang, J. Mei, R. Hu, J. Z. Sun, A. Qin and B. Z. Tang, *J. Am. Chem. Soc.*, 2012, **134**, 9956–9966; (*b*) M. P. Aldred, C. Li, G.-F. Zhang, W.-L. Gong, A. D. Q. Li, Y. Dai, D. Ma and M.-Q. Zhu, *J. Mater. Chem.*, 2012, **22**, 7515–7528; (*c*) J. Li, Y. Duan and Q. Li, *Dyes Pigm.*, 2013, **96**, 391–396; (*d*) J. Huang, N. Sun, J. Yang, R. Tang, Q. Li, D. Ma, J. Qin and Z. Li, *J. Mater. Chem.*, 2012, **22**, 12001–12007; (*e*) N. B. Shustova, B. D. McCarthy and M. Dinca, *J. Am. Chem. Soc.*, 2011, **133**, 20126–20129; (*f*) P. P. Kapadia, L. R. Ditzler, J. Baltrusaitis, D. C. Swenson, A. V. Tivanski and F. C. Pigge, *J. Am. Chem. Soc.*, 2011, **133**, 8490–8493; (*g*) J. Huang, D. Wu, H.-J. Ge, S.-H. Liu and J. Yin, *Chin. Chem. Lett.*, 2014, **25**, 1399–1402.

2 (*a*) X. Gu, G. Zhang, Z. Wang, W. Liu, L. Xiao and D. Zhang, *Analyst*, 2013, **138**, 2427–2431; (*b*) X. Chen, X. Y. Shen, E. Guan, Y. Liu, A. Qin, J. Z. Sun and B. Z. Tang, *Chem. Commun.*, 2013, **49**, 1503–1505; (*c*) S. Song and Y.-S. Zheng, *Org. Lett.*, 2013, **15**, 820–823.

3 (*a*) X. Wang, J. Hu, T. Liu, G. Zhang and S. Liu, *J. Mater. Chem.*, 2012, **22**, 8622–8628; (*b*) N.-N. Liu, S. Song, D.-M. Li and Y.-S. Zheng, *Chem. Commun.*, 2012, **48**, 4908–4910; (*c*) Z.-Y. Li, W. Xue, G.-X. Liu, D. Wu, T.-T. Li, S.-H. Liu and J. Yin, *Chin. Chem. Lett.*, 2013, **24**, 189–191; (*d*) B. Xu, X. Wu, H. Li, H. Tong and L. Wang, *Macromolecules*, 2011, **44**, 5089–5092.

4 (*a*) W. Z. Yuan, Z.-Q. Yu, Y. Tang, J. W. Y. Lam, N. Xie, P. Lu, E.-Q. Chen and B. Z. Tang, *Macromolecules*, 2011, **44**, 9618–9628; (*b*) Y. Q. Dong, J. W. Y. Lam and B. Z. Tang, *J. Phys. Chem. Lett.*, 2015, **6**, 3429–3436.

5 (*a*) R. T. K. Kwok, J. Geng, J. W. Y. Lam, E. Zhao, G. Wang, R. Zhan, B. Liu and B. Z. Tang, *J. Mater. Chem. B*, 2014, **2**, 4134–4141; (*b*) D. Ding, J. Liang, H. Shi, R. T. K. Kwok, M. Gao, G. Feng, Y. Yuan, B. Z. Tang and B. Liu, *J. Mater. Chem. B*, 2014, **2**, 231–238; (*c*) Q. Wan, M. Liu, D. Xu, H. Huang, L. Mao, G. Zeng, F. Deng, X. Zhang and Y. Wei, *J. Mater. Chem. B*, 2016, **4**, 4033–4039.

6 J. Luo, Z. Xie, J. W. Y. Lam, L. Cheng, H. Chen, C. Qiu, H. S. Kwok, X. Zhan, Y. Liu, D. Zhu and B. Z. Tang, *Chem. Commun.*, 2001, 1740–1741.

7 (*a*) R. T. K. Kwok, C. W. T. Leung, J. W. Y. Lam and B. Z. Tang, *Chem. Soc. Rev.*, 2015, **44**, 4228–4238; (*b*) Y. Hong, J. W. Y. Lam and B. Z. Tang, *Chem. Soc. Rev.*, 2011, **40**, 5361–5388; (*c*) D. Ding, K. Li, B. Liu and B. Z. Tang, *Acc. Chem. Res.*, 2013, **46**, 2441–2453; (*d*) Y. Hong, J. W. Y. Lam and B. Z. Tang, *Chem. Commun.*, 2009, 4332–4353; (*e*) D. Ding, J. Liang, H. Shi, R. T. K. Kwok, M. Gao, G. Feng, Y. Yuan, B. Z. Tang and B. Liu, *J. Mater. Chem. B*, 2014, **2**, 231–238; (*f*) G. Zhang, F. Hu and D. Zhang, *Langmuir*, 2015, **31**, 4593–4604.

8 (*a*) J. Mei, N. L. C. Leung, R. T. K. Kwok, J. W. Y. Lam and B. Z. Tang, *Chem. Rev.*, 2015, **115**, 11718–11940; (*b*) R. Hu, Y. Kang and B. Z. Tang, *Polym. J.*, 2016, **48**, 359–370; (*c*) P.-C. Shen, Z.-Y. Zhuang, Z.-J. Zhao and B. Z. Tang, *Chin. Chem. Lett.*, 2016, **27**, 1115–1123.

9 (*a*) Y. Yang, C.-Y. Gao and T. Li, *ChemistrySelect*, 2016, **1**, 4577–4581; (*b*) A. Ozawa, A. Shimizu, R. Nishiyabu and Y. Kubo, *Chem. Commun.*, 2015, **51**, 118–121; (*c*) R. Singh, A. K. Dwivedi, A. Singh, C.-M. Lin, R. Arumugaperumal, K.-H. Wei and H.-C. Lin, *ACS Appl. Mater. Interfaces*, 2016, **8**, 6751–6762; (*d*) Z. Ma, Z. Wang, X. Meng, Z. Ma, Z. Xu, Y. Ma and X. Jia, *Angew. Chem., Int. Ed.*, 2016, **55**, 519–522; (*e*) Y. Yang, C.-Y. Gao, N. Zhang and D. Dong, *Sens. Actuators, B*, 2016, **222**, 741–746; (*f*) Y. Yuan, C.-J. Zhang, S. Xu and B. Liu, *Chem. Sci.*, 2016, **7**, 1862–1866.

10 E. Şen, K. Meral and S. Atılgan, *Chem. – Eur. J.*, 2016, **22**, 736–745.

11 Y. Yuan, R. T. K. Kwok, G. Feng, J. Liang, J. Geng, B. Z. Tang and B. Liu, *Chem. Commun.*, 2014, **50**, 295–297.

12 (*a*) Y. Zhang, H. Chen, D. Chen, D. Wu, Z. Chen, J. Zhang, X. Chen, S. H. Liu and J. Yin, *Sens. Actuators, B*, 2016, **224**, 907–914; (*b*) X. Han, M. Cao, Z. Xu, D. Wu, Z. Chen, A. Wu, S. H. Liu and J. Yin, *Org. Biomol. Chem.*, 2015, **13**,

9767–9774; (*c*) Y. Zhang, H. Chen, D. Chen, D. Wu, X. Chen, S. H. Liu and J. Yin, *Org. Biomol. Chem.*, 2015, **13**, 9760–9766; (*d*) G. Liu, D. Wu, J. Liang, X. Han, S. H. Liu and J. Yin, *Org. Biomol. Chem.*, 2015, **13**, 4090–4100; (*e*) M. Cao, L. Jiang, F. Hu, Y. Zhang, W. C. Yang, S. H. Liu and J. Yin, *RSC Adv.*, 2015, **5**, 23666–23670; (*f*) F. Hu, M. Cao, J. Huang, Z. Chen, D. Wu, Z. Xu, S. H. Liu and J. Yin, *Dyes Pigm.*, 2015, **119**, 108–115.

13 X. Liu, Q. Qiao, W. Tian, W. Liu, J. Chen, M. J. Lang and Z. Xu, *J. Am. Chem. Soc.*, 2016, **138**, 6960–6963.

14 S.-Y. Parka, M. Ebiharab, Y. Kubotaa, K. Funabikia and M. Matsui, *Dyes Pigm.*, 2009, **82**, 258–267.